ADVANCED SUSTAINABLE SYSTEMS
www.advsustainsys.com

A Transient Spore-Forming Microbial Fuel Cell with Extracellularly Biosynthesized Tin Oxide Nanoparticles for Powering Disposable and Green Papertronics

*Maryam Rezaie, Zahra Rafiee, and Seokheun Choi**

Transient electronics, which can operate only for short-lived applications and then be eco-friendly disintegrated, create opportunities in environmental sensing, healthcare, and hardware security. Paper-based electronics, or papertronics, recently have rapidly advanced the physically transient device platform because paper as a foundation offers an environmentally sustainable and cost-effective option for those increasingly pervasive and fast-updated single-use applications. Paper-based power supplies are indispensable to realize a fully papertronic paradigm and are a critical enabler of environmentally benign power solutions. Microbial fuel cells (MFCs) hold great potential as power sources for such green papertronic applications. This work reports the design, operation, and optimization of a high-power papertronic MFC by biosynthesizing microbe-mediated tin oxide nanoparticles (SnO_2 NPs) on dormant Bacillus subtilis endospores. They form an electrical conduit that improves electron harvesting during the spore germination and power generation. The MFC is packaged in a sub-microporous alginate to minimize the potential risk of bacteria leakage. Upon the introduction of water, the paper-based MFC generates a significantly enhanced power density of 140 μW cm^{-2}, which is more than two orders of magnitude greater than their previously reported counterparts. Six MFCs connected in series generate more than sufficient power to run an on-chip, light-emitting diode.

1. Introduction

Paper-based electronics or papertronics is a new scheme of electronics that is revolutionarily constructed on a disposable and green paper substrate to offer emerging short-term applications and ensure minimal environmental effects upon disposal.[1,2] Papertronics have been exclusively designed for a single-use operation, especially in point-of-care diagnostics or for a predefined duration in shipment tracking, environmental sensing, and food and grocery monitoring.[3,4] Then, the biocompatible, combustible paper can be disposed of by allowing ambient microorganisms in the soil to disintegrate the device or through the more proper disposal method of incineration.[5–7] Many passive (e.g., resistors, capacitors, and inductors) and active (e.g., transistors and operational amplifiers) electronic components have been successfully fabricated on top of or within paper.[2,8–11] Even multilayer printed circuit boards (PCBs) were manufactured on paper substrates with various forms of vias, offering new opportunities for more complicated and high-end functional circuits.[12,13] Although its performance and applications are not yet comparable to conventional integrated electronics,[2] disposable and biocompatible all-paper-based devices have received increasing attention while electronic waste, or e-waste, is the fastest-growing global waste stream in the world with projections estimating almost 75 million tons per year by 2030.[14,15] To this end, green materials and processing that minimize environmental risks are being considered for the manufacturing of paper-based electronics while reducing cost and improving performance have been simultaneously pursued.[1,2,5]

Despite excitement about this conceptual paradigm for electronics, our ability to harness the potential of papertronic technology lags from a lack of power solution that can realize a truly stand-alone device platform.[4,16–19] For fully independent, integrated, and self-sufficient devices, the power source as part of the papertronics must have the same eco-friendliness, low-cost, disposability, and biodegradability. Many paper-based batteries and energy storage devices have been developed as discrete power components for conventional electronics by exploiting paper's outstanding features such as inexpensiveness, flexibility, lightweight, and large surface area.[17] The batteries include electrochemical batteries, Lithium-ion batteries, solar cells, supercapacitors, and nanogenerators. However, those batteries were

M. Rezaie, Z. Rafiee, S. Choi
Bioelectronics & Microsystems Laboratory
Department of Electrical & Computer Engineering
State University of New York at Binghamton
Binghamton, NY 13902, USA
E-mail: sechoi@binghamton.edu

S. Choi
Center for Research in Advanced Sensing Technologies & Environmental Sustainability
State University of New York at Binghamton
Binghamton, NY 13902, USA

The ORCID identification number(s) for the author(s) of this article can be found under https://doi.org/10.1002/adsu.202300357

DOI: 10.1002/adsu.202300357

not designed as a fully integrated power source for self-powered papertronics and most previously-developed paper batteries can hardly be considered environmentally benign.[20] Usually, batteries are the most problematic waste because they require toxic reactive materials and energy-intensive or non-eco-friendly manufacturing processes.[21]

Recently, paper-based microbial fuel cells (MFCs) served as eco-friendly integrated papertronic biobatteries where preloaded microorganisms convert supplied organic matter to electricity through microbial metabolism until the matter is depleted.[18,19,22] Because of the eco-friendliness of the microorganisms as a biocatalyst, the simplicity of the device configuration, and the biodegradability of such device components as graphite-based electrodes and conductive organic polymers, the paper-based MFCs are gaining acceptance as a power solution for the disposable and green papertronics.[23,24] Moreover, the organic substrates can be pre-integrated within the paper MFC in a dry form, which will enable battery compatibility with the solid-state papertronic systems.[25,26] Even, the microorganisms can be pre-inoculated in a freeze-dried format so that the microbial viability can be maintained until needed.[4,19] Very recently, our group revolutionized the shelf-life of the MFC by using endospores as a dormant biocatalyst and successfully demonstrated its power generation by germinating the spores with specific nutrients.[27,28] All solid-phase MFC components and the hygroscopic nature of paper allowed simple power generation with water introduction or moisture harvested from the air.[28] If sufficient power can be produced, spore-forming MFCs will become the best-fit power source for the manufacture and operation of papertronic systems because they exploit the robust nature of bacterial spores for processing and prolonged storage. Existing paper-based MFCs are very limited by their low power (≈1 μW cm^2) and short shelf-life (≈a couple of hours), which renders them insufficient for practical applications.[4,19] The latest advances in spore-forming MFCs on paper were much worse in power generation (≈0.5 μW cm^{-2}) even though they significantly improved the shelf-life (≈ a month).[26] This is because the endospores used belong to Gram-positive bacteria which usually have a very thick cell membrane, impeding the extracellular electron transfer during their metabolism.[29]

In this work, we provide barrier-transcending bioelectricity generation from a Gram-positive spore-forming MFC developed on paper by extracellularly biosynthesizing tin oxide (SnO_2) nanoparticles on the surface of the endospores. When the endospores germinate, the nanoparticles electronically or electrochemically connect the cells with an external anode, considerably improving the extracellular transfer efficiency of the electrons through the thick and insulating cell membrane. The biogenic SnO_2 nanoparticles are biocompatible, and manufactured in an eco-friendly and cost-effective manner. During the biosynthetic reduction of a chemical solution including tin ions, bacterial sporulation is triggered by unfavorable environmental conditions. This avoids additional steps to prepare the dormant endospores as the biocatalyst for the MFC. Impressively, the maximum power density of the paper MFC with SnO_2 nanoparticles achieved 140 μW cm^{-2}, which was more than two orders of magnitude greater than the previously-reported counterparts. By integrating six MFCs into a single sheet of paper and serially connecting them through folding, 1.75 V of the open circuit voltage and 128 μW of the output power were achieved, powering an on-chip, light-emitting diode. The operational voltage of single-use biomedical devices like glucometers, pulse oximeters, electrocardiogram (ECG) monitors, and point-of-care devices typically falls within the range of 1.2–1.5 V. These devices often use low-power electronic components and small batteries to provide the necessary voltage for their operation. Fortunately, our paper-based MFCs meet the necessary criteria to serve as a viable power source for these biomedical devices.

2. Results and Discussion

2.1. Biocatalytic Endospores with Extracellularly Biosynthesized SnO_2 Nanoparticles

An MFC requires three functional components to operate: an anode with biocatalysts, an ion-exchange membrane, and a cathode with catalysts.[22–24] When an organic source is available for the metabolism of the microbial biocatalyst, a redox metabolic reaction occurs generating electrons and protons. The electrons move along an external circuit powering a load while the protons travel internally through the ion-exchange membrane. At the cathode, the catalytic reaction accepts the electrons and protons, allowing the MFC operation. Conventional MFCs use rigid substrates to define the electrodes and a chamber to include aquatic biocatalysts and organic sources, complicating device fabrication.[22] Usually, the microbial biocatalysts are prepared two-dimensionally on the rigid anode by forming a biofilm, which requires a significant starting time for power generation. Recently, MFCs have been simply constructed on paper.[18,19] Individual layers of paper can be functionally engineered to be each MFC component or the entire MFC can be three-dimensionally constructed within a single sheet of paper by being folded. Because of its hydrophilic properties, paper facilitates the adhesion of microbial cells in a liquid to its intertwined fiber network. Paper allows 3D biofilm formation through its porous structure, reducing the starting time for power generation along significantly enhancing performance. Moreover, the use of endospores as biocatalysts opened a broad avenue for paper-based MFCs by substantially improving their shelf-life and manufacturing.[26] Some types of bacteria such as *Bacillus subtilis (B. subtilis)* can transform their bodies into dormant and durable endospores in adverse environmental conditions and survive storage for many years without losing their viability.[30] Moreover, because the spore form can tolerate external stresses such as hot/cold temperature, high pressure, and desiccation, they can be readily used as a durable material for microfabrication.[31] When the conditions become favorable, the endospores return to a metabolically active state through germination and generate power. Those conditions can be simply controlled with nutrients where the sporulation can be triggered by nutrient depletion and the germination can be provoked by special germinants.[30] Despite the successful demonstration of power production through the germination of *B. subtilis* spores and their extended shelf-life,[26] the actual application of the spore-forming MFC on paper has been very limited because of its extremely low power. *B. subtilis* is a very weak electrogenic species because of its thick and potentially insulating cell membrane.[32]

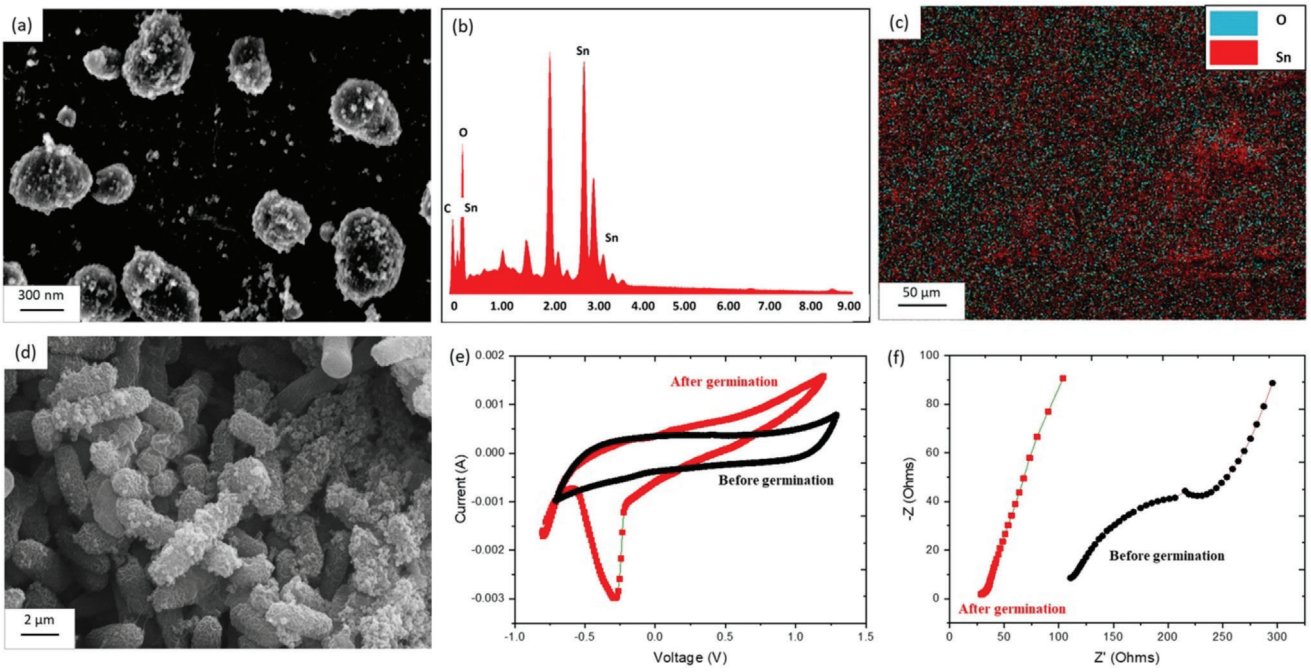

Figure 1. a) SEM image of *B. subtilis* endospores with biosynthesized SnO2 NPs, b) EDS spectrum of the NPs, c) EDX mapping of elements O and Sn in SnO2, d) SEM image of germinated *B. subtilis* with biosynthesized SnO2 NPs, e) CV profiles and f) EIS spectra in 0.1 M KCl at scan rate 100 mV s^{-1} of the NP-decorated *B. subtilis* endospores before and after germination.

In this work, we propose tin oxide nanoparticles (SnO_2 NPs) extracellularly biosynthesized on the *B. subtilis* endospores as an electrical conduit to radically improve the electron transfer rate through the cell membrane. Previously, the conjugation of artificial NPs with microbial biocatalysts provided an innovative means to promote electron transfer efficiency and improve the power generation of the MFC.[33,34] However, the general fabrication of NPs requires energy-intensive toxic processes with harmful chemicals, and the coupling with microbes is very complicated.[35] Although even in situ formation of NPs directly within the microbes by using their redox activities was successfully demonstrated as a biocompatible approach with MFC manufacturing and operation,[35,36] the concept of the MFCs with NPs was not suitable for general long-term energy and environmental applications. This is because the NPs cannot be used by the following generations of microbes,[35] limiting their practical long-term operation. However, biosynthetic NPs would be beneficial exclusively for single-use or short-term operations as sufficient power generation can be extracted for those transient applications before the microbes reproduce. Moreover, the eco-friendly, cost-effective, and in situ bottom-up synthetic approach can be synergistic with disposable and green papertronic technology. In particular, SnO_2 NPs are a promising electron pathway for boosting microbial electricity production because they are very conducting and have a large surface-to-volume ratio.[37,38] Their strong chemical and physical interactions with other materials make SnO_2 NPs a favorable candidate for many other energy-producing devices. Moreover, their strong thermal stability (up to 500 °C) can improve the storage capability along with the enduring endospores. Here, SnO_2 NPs were, for the first time, biosynthesized directly on the surface of *B. subtilis* endospores, through their bioelectrochemical reduction of a Tin (II) chloride solution, $SnCl_2$. When the vegetative *B. subtilis* cells were in the $SnCl_2$ solution, the positively charged Sn^{2+} ions were attracted by the negatively charged cell wall and then the bacterial electrochemical activity converted those ions to NPs (Figure S1, Supporting Information). Additionally, other organic functional molecules such as hydroxyl groups (—OH), carboxyl groups (—COOH), or amine groups ($—NH_2$) can reduce ions to NPs.[39] Eventually, the oxygen available in the solution oxidized the NPs to turn into SnO_2 NPs. Notably, during biosynthesis, the vegetative cells simultaneously become endospores to survive and adapt at high concentrations of metallic solutions. This direct transformation of the *B. subtilis* cells into dormant spores with SnO_2 NPs helped streamline biocatalyst preparation by eliminating the complicated, time-consuming, and labor-intensive sporulation process.[40] Scanning electron microscopy (SEM) showed that NPs of various sizes formed on the spores (**Figure 1**a). In the SEM images, dark cells in biological samples result from complex, dense surfaces that absorb or scatter high-energy electrons, emitting fewer secondary electrons. In contrast, bright SnO_2 nanoparticles emit more secondary electrons due to their smaller size and potentially lower density, resulting in a brighter appearance (Figure S2, Supporting Information). An Energy Dispersive X-ray (EDX) microanalysis displayed the signals from Sn and O, revealing the presence of SnO_2 NPs (Figure 1b). The EDX mapping illustrated extensive dispersion of Sn and O elements, confirming that they are well-distributed (Figure 1c). Figure S3 (Supporting Information) illustrates the Fourier-transform infrared spectroscopy (FTIR) findings for the decorated spore bacteria, highlighting the differentiation between spores before and after the decoration process. The significantly higher transmittance percentage and increased peak

intensity were observed in *B. subtilis* spores decorated with SnO_2 NPs compared to pristine *B. subtilis* spores. Tin SnO_2 NPs often have lower infrared (IR) absorption and can scatter incident IR light less, leading to reduced absorption of IR radiation. Additionally, surface modifications and interactions between the nanoparticles and spores can alter the spore's IR absorption behavior, potentially enhancing spectral features and increasing peak intensity. This interaction may also dilute the sample or reduce its thickness, contributing to higher transmittance percentages. the spherical-shaped spores were exposed to a specific chemical germinant, a mixture of *L*-Valine and AGFK (*L*-Aspargine, *D*-glucose, *D*-fructose, and K^+ ions), they transitioned into the rod-shaped vegetative cells while the SnO_2 NPs were retained on the surface of the cells (Figure 1d). The *B. subtilis* germination process is generally involved with three germinant receptors, GerA, GerB, and GerK.[30] The GerA receptor recognizes *L*-Valine for germination while the GerB and GerK respond to AGFK.

Cyclic voltammetry (CV) measurements in a three-electrode electrochemical cell at a scan rate of 100 mV s^{-1} showed significant electrochemical activity from the vegetative cells through the SnO_2 NPs while the spores did not develop any redox processes (Figure 1e). A scan rate of 100 mV s^{-1} was selected due to its standard parameter in electrochemical studies, enabling easy comparisons with existing research and providing a balance between data quality and experimental efficiency. *B. subtilis* spores typically lack oxidation and reduction peaks due to their dormant, metabolically inactive state, characterized by limited redox activity. However, upon germination and activation of metabolic processes, these spores undergo significant biochemical transformations. This shift triggers the emergence of oxidation and reduction peaks as redox-active molecules become more abundant and engage in electrochemical reactions, marking the transition from dormancy to metabolic activity. The presence of SnO_2 NPs on the spore surface plays a pivotal role as electron transfer mediators and catalysts, significantly enhancing electron transfer and catalyzing redox reactions (Figures 1e; Figure S4, Supporting Information). That interaction with the NPSs further contributes to the appearance of the reduction peak in the CV curves following the germination of *B. subtilis* spores.

The redox curves of the vegetative cells with the NPs were very stable even after 20 cycles, which is indicative of a robust and reliable electrochemical performance (Figure S5, Supporting Information). The electrochemical impedance spectroscopy (EIS) experiments demonstrated that the germinated cells significantly improved the electron transfer efficiency through the NPs during their metabolic activity (Figure 1f).

2.2. Design, Operation, Performance, and Optimization of the Paper-Based MFC

To characterize the suitability of the NP-coated spores as a dormant biocatalyst for papertronics, we developed a paper-based MFC that would be readily integrated into the other papertronic systems. A 3D MFC was constructed from a 2D sheet of paper that incorporated the anode, cathode, and ion exchange membrane. Hydrophilic regions were first defined for those individual MFC components by hydrophobic wax patterning. Hydrophilic regions were further processed to be highly conductive for the anode and electrocatalytic for the cathode. Partial wax penetration through the cathode allowed the formation of an ion exchange membrane. In the engineered anodic compartment, the endospores with the biogenic SnO_2 NPs were loaded as a dormant biocatalyst. The MFC was easily formed by folding the paper along a pre-defined crease and putting the three essential components together vertically. To activate the MFC, we introduced the germinant organic matter, a mixture of *L*-Valine and AGFK in a Luria Broth (LB) medium, and waited for an hour for the maximum spore germination. Then, the MFC was run in an open-circuit mode and its open-circuit voltage (OCV) was monitored to characterize the initial MFC performance. Usually, the OCV in the MFC reflects the thermodynamic activities of biocatalysts in oxidizing organic matter against the cathodic potential, indicating the overall power-producing capability. A high OCV value (Red square in **Figure 2**d) was obtained as the spores with the NPs germinated (Figure S6a, Supporting Information), which was significantly larger than that of the counterpart without the NPs (Black star in Figure 2d). Their OCV values gradually decreased as the organic matter was depleted through the bacterial metabolic reaction. When we simply dropped LB without the germinant on the dormant bacteria, the spores barely germinated (Figure S6b, Supporting Information) and produced very negligible abiotic electricity (Blue circle in Figure 2d), which originated from transient NP activity with the organic chemicals. The germinant itself without the spore biocatalysts did not generate any meaningful OCV value (Pink triangle in Figure 2d).

To thoroughly evaluate the electrogenic capability of the biocatalysts and the effect of the biosynthetic process on the power generation, multiple MFCs were prepared with various biocatalytic samples which were biosynthesized with different concentrations of bacteria and metal ion solutions for the NP biosynthesis. First, the concentration of the Tin (II) chloride solution changed (no solution, 0.5, 1, 1.5, and 2 mg L^{-1}) for the biosynthesis of the SnO_2 NPs while the bacterial concentration was fixed with an optical density value at 600 nm (OD_{600}) of 1.5. The concentration of 1.5 OD_{600} corresponds to 2.25×10^8 colonies of *B. subtilis* per mL. During the biosynthesis, the cells became endospores with the NPs on their cell membrane. When the germinants were introduced into the paper MFCs, the polarization curves (i.e., the voltage output for a given current density) and power densities were measured through various external resistors (**Figure 3**a). The MFC with the NPs synthesized in 1 mg L^{-1} $SnCl_2$ generated the highest OCV and power density (Figure 3b,c). Similarly, the NPs were biosynthesized with different bacterial concentrations (i.e., 1, 1.5, 2, 2.5, and >3 OD_{600}) while the concentration of $SnCl_2$ was adjusted to be constant with 1 mg L^{-1}. One hour after the germinant introduction, the polarization curves and power densities of the MFCs were obtained (Figure 3d). The MFC with 1.5 OD_{600} sample produced the highest OCV and power density (Figure 3e,f). The concentration of the bacteria and metal ion solution during the biosynthesis substantially affected the MFC power performance. Although further study is needed to quantify the amount and the size of the NPs according to their concentrations, we assume that the higher concentration of tin in the solution compared to the number of bacteria can negatively affect the bacterial viability while the lower $SnCl_2$ concentration can produce fewer NPs.[41,42] The best electrical performance was obtained with 1.5 OD_{600} and 1 mg L^{-1} $SnCl_2$,

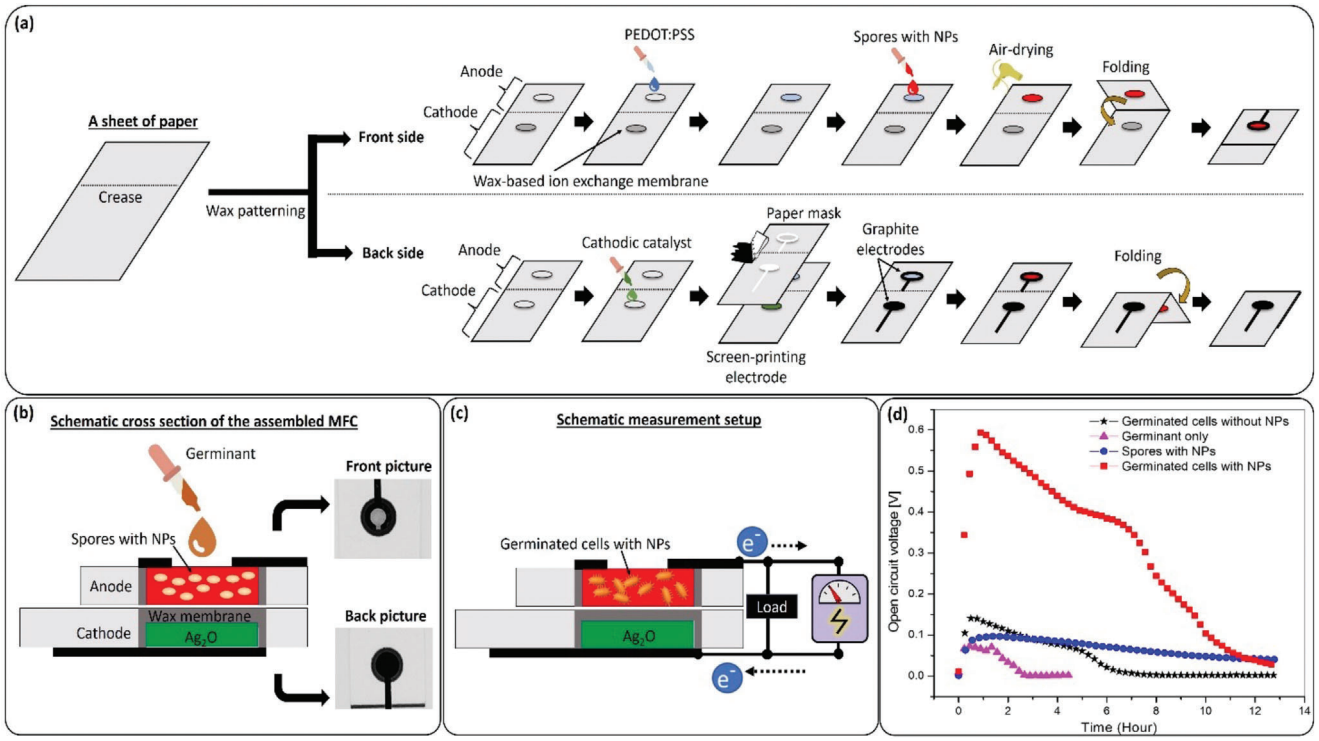

Figure 2. a) Overview of the single MFC fabrication–integration of the device components into a single sheet of paper and origami-based folding of the 2D sheet to form a 3D MFC, b) schematic cross-section diagram and pictures of the front and back of the assembled MFC, c) schematic measurement setup after a germinant is introduced, and d) Continuous measurement of the open circuit voltages with various biocatalytic samples; germinant only, spores with the NPs, and germinated cells with and without the NPs.

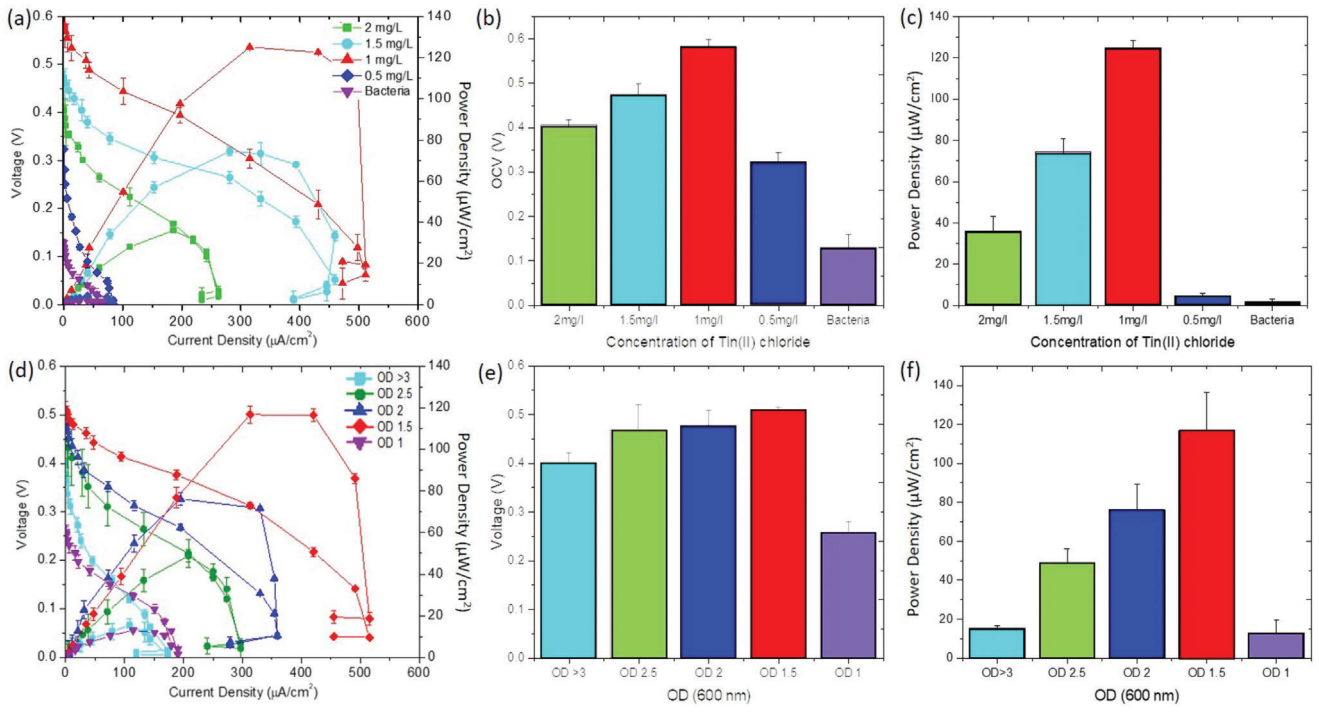

Figure 3. a) Polarization curves and power outputs, b) OCVs, c) Maximum power densities of the MFCs with the NPs biosynthesized in different concentrations of the $SnCl_2$ solution (Bacterial concentration is fixed at 1.5 OD_{600}). d) Polarization curves and power outputs, e) OCVs, f) Maximum power densities of the MFCs with the NPs biosynthesized in different concentrations of the bacterial cells ($SnCl_2$ concentration is fixed at 1.0 mg L^{-1}).

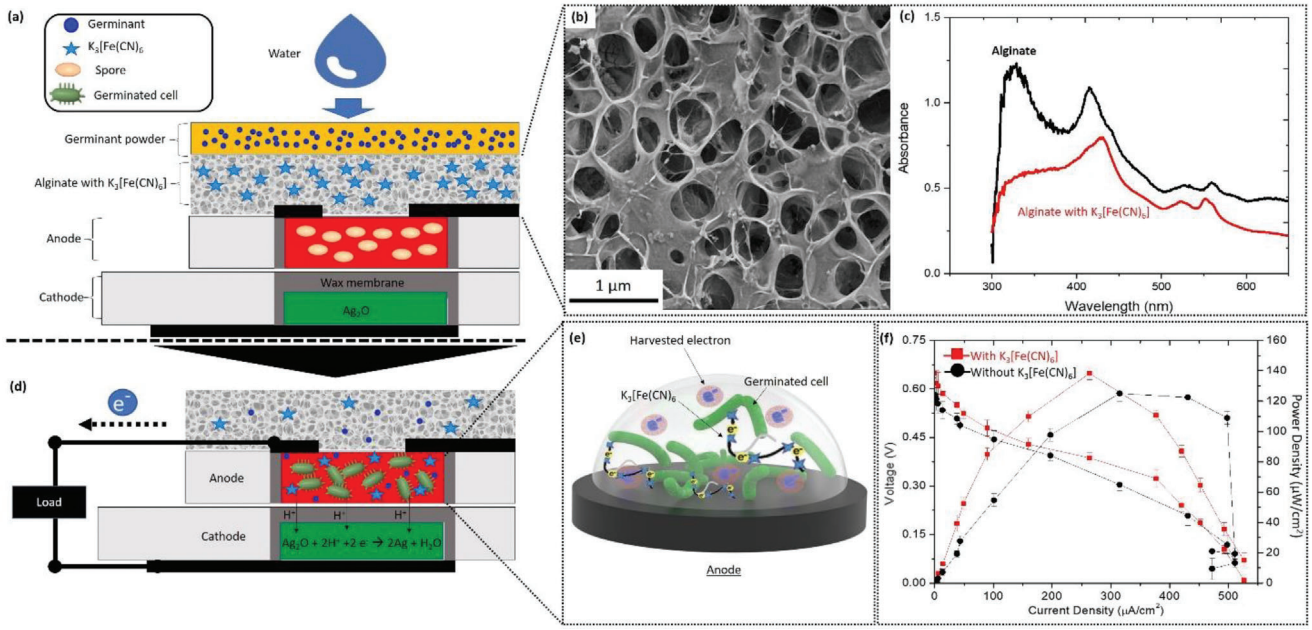

Figure 4. a) Conceptual image of the paper-based MFC packaged with sub-microporous and electrochemical-mediated alginate with a nutrient germinant. The MFC can be activated by a water introduction for on-demand power generation. b) SEM image of the alginate. c) UV–vis spectra of the alginate with and without $K_3Fe(CN)_6$. Schematic illustrations of d) the MFC operating with a water droplet and e) the extracellular electron transfer facilitated by the $K_3Fe(CN)_6$. f) Polarization curves and power outputs of the MFCs with and without $K_3Fe(CN)_6$.

producing a power density of ≈120 μW cm^{-2}. Those optimized concentrations were used for all the experiments throughout this work. We need to emphasize that spores in a dormant state maintain limited metabolic activity and do not actively participate in the electrogenic processes crucial for power generation. Their durability ensures safety and reliability, as they can be stored until needed, making *B. subtilis* a practical choice for various environmental contexts and applications like MFCs.

2.3. A Biobattery Covered by Sub-Microporous and Electrochemical-Mediated Alginate with a Nutrient Germinant

Practical paper-based MFCs as a portable power source for actual papertronic applications can be realized when on-demand power can be readily activated and the devices can be safely operated. Although the biocatalysts we used are considered a group generally recognized as safe (GRAS), they need to remain in the device to avoid potential health and environmental threats. Here, the anode possessing the biocatalysts was carefully covered by a hydrophilic, porous alginate-based hydrogel (**Figure 4**a). The size of the pores is below 1 μm in diameter, effectively preventing the rod-shaped vegetative cells and even the round-shaped spores from moving out of the MFC and posing any negative concerns (Figure 4b). The mean diameter of the *B. subtilis* spore is ≈1.3 μm with an aspect ratio of 1.86 while the size of the vegetative cell is much larger than the spore. To further increase the efficiency of the extracellular electron transfer from the cells to the conductive network of the engineered paper, potassium ferricyanide ($K_3Fe(CN)_6$) was included in the alginate packaging layer. Potassium ferricyanide is a promising mediator for weak exoelectrogens to improve the interactions between the biocatalysts and the electrode.[43] The presence of the mediator in the alginate was confirmed from the UV–vis spectra where the wide UV absorption band between 300 and 350 nm because of the conjugated double bonds of alginate disappear with the addition of the mediator (Figure 4c). The disappearance of the UV-visible absorption peak could be attributed to both the oxidation of alginate and a chemical reaction. $K_3Fe(CN)_6$ has the potential to oxidize certain functional groups within alginate, inducing structural alterations that cause the 350 nm peak to disappear. Additionally, $K_3Fe(CN)_6$ might engage specific functional groups in alginate, resulting in the creation of novel chemical compounds. This chemical transformation could modify the molecule's structure, consequently influencing its UV–vis absorption characteristics.

On top of the gluey and sticky hydrogel, dried germinant-included LB powders were readily drop-casted and tightly attached (Figure 4a). This compound-integrated MFC allowed on-demand power generation by simply dropping a single drop of water. When the droplet of water was introduced onto the device, it penetrated through the germinant and packaging layers by capillary action of the hydrophilic alginate and the paper and delivered the germinant-included organic matter and the mediators down to the endospores in the anodic layer (Figure 4d). That allowed spore germination and power production with improved electron transfer efficiency. The mediator uses diffusive transport to effectively deliver the metabolically produced electrons to the electrode in its reduced state while the mediator diffuses back to the biocatalyst in its oxidized state, allowing continuous electron transfer (Figure 4e). The use of the mediator increased the OCV and power density (Figure 4f).

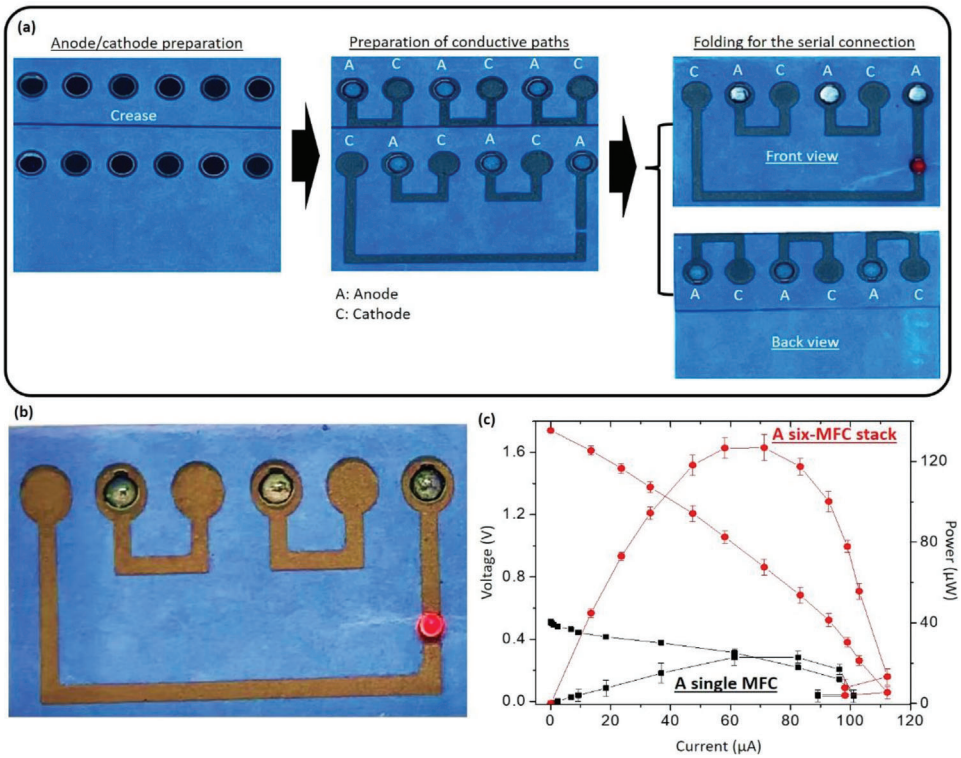

Figure 5. a) Overview of the six-MFC stack fabrication, b) the stack with the LED on, and c) polarization curves and power outputs of the single MFC and the six-MFC stack.

2.4. A Portable, High-Power MFC Stack for Disposable and Green Papertronics

The fusion of the art of origami and papertronic technology allowed MFCs to be integratable, scalable, and batch-fabricable. The configuration and fabrication techniques of our single MFC were applied to construct in-series-connected MFCs stacked on a single sheet of paper. Six MFCs incorporated into the 2D sheet were directly connected in series by folding along the defined crease (**Figure 5**a; Figures S7 and S8 , Supporting Information). Metallic paths were prepared by spraying nickel, creating the printed circuit board (PCB) on paper to connect the MFCs. A light-emitting diode (LED) was mounted on the PCB as a model on-chip application. One hour after introducing droplets on the six anodes, the MFC stack produced sufficient power to turn on the LED (Figure 5b; Movie S1, Supporting Information). Compared with the single MFC, the stack significantly enhanced output voltage and power (Figure 5c). The maximum power of 128 μW in the stack surpassed 20 μW for the single MFC by a factor of 6.2. The OCV of the stack was ≈1.75 V, which was much higher than that of the single MFC. These results indicate that a series connection of multiple MFCs was successfully established in this paper-based platform. However, the OCV of the stack averaged 0.291 V per cell and developed a loss of 0.209 V compared to the OCV of the single MFC (≈0.5 V). Such voltage loss at the open circuit can be attributed to a parasitic electric current passing through the metallic paths between the adjacent MFCs, which has been noticed in previous reports.[44,45] In the future, to minimize the parasitic current, we may disconnect the individual units before the stack is operated.

One of the most important requirements for single-use papertronic devices is biodegradability. This aspect is more important for single-use energy-producing devices because their essential non-biodegradable components can generate toxic and hazardous wastes. Unlike many conventional paper-based power sources and batteries, one advantage of paper-based MFCs is their easily biodegradable nature. During biodegradation, a large weight loss from a paper-based single MFC in a bacterial culture of *B. subtilis* was observed within only 3 weeks (**Figure 6**a,b). The cellulose paper as the device foundation and the bacterial cells as the energy catalysts are fully biodegradable while the other materials including the PEDOT:PSS, biogenic NPs, and graphite are considered biocompatible. Even inorganic nickel for the metallic paths and silver oxide for cathodic reactions could be bioremediated by the electrochemically active bacteria, *B. subtilis*. Although studies are needed to investigate the bioremediation of those materials in paper, many reports demonstrate microbial bioremediation.[21,46,47] When our paper-based MFC stack was buried in natural soil, it became fractured and biodegraded after three weeks (Figure 6c).

3. Conclusion

Here, we developed a high-performance MFC on paper by biosynthesizing SnO_2 NPs on biocatalytic bacterial cells. The NPs served as an electrical conduit to improve the extracellular

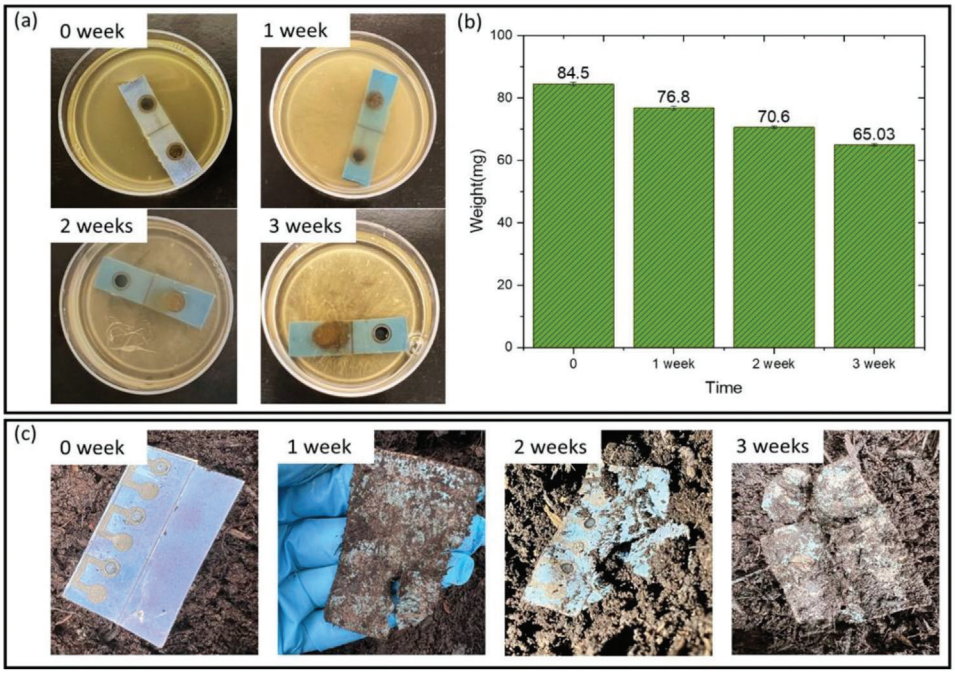

Figure 6. Biodegradability test. a) Photoimages of the degradation process for a paper-based single MFC in a bacterial culture of *B. subtilis* and b) its weight loss. c) Photo images of the biodegration process for a paper-based MFC stack in natural soil.

electron transfer from the cells to an external electrode. During the biosynthesis, the vegetative *B. subtilis* created the NPs through electrochemical reduction while becoming endospores by using their adaptive strategy to survive in toxic chemical conditions. The NPs-coated endospores were used as dormant biocatalysts in the MFC that revived to generate power upon the nutrient introduction. The MFC was packaged in a sub-microporous and electrochemical-mediated alginate with a nutrient germinant so that the biocatalysts can be contained, which protects the MFC and prevents leakage of toxic waste. The packaging provides redox mediators, which enhance power production. Moreover, the pre-loaded germinant allowed on-demand power generation with a simple water introduction. A single MFC generated a much higher power density, 140 μW cm^{-2}, than all previously reported paper-based MFCs. By integrating six MFCs into a single sheet of paper and connecting them in series through metallic paths sprayed on the same substrate, an on-chip LED was successfully turned on, ensuring the practical efficacy of this power technique for self-powered papertronic operations. Moreover, the paper-based MFC biodegraded, indicating that it can be very suitable as a power source for disposable and green papertronic applications while reducing e-waste.

4. Experimental Section

Bacillus Subtilis (B. Subtilis) Inoculums: The *B. subtilis* strain 168 obtained from the American Type Culture Collection (ATCC) was first cultured in a Luria Broth (LB) medium with gentle shaking for 24 h at 37 °C. The growth of *B. subtilis* was monitored at the optical density of 600 nm (OD_{600}). When the OD_{600} reached 3.0, the cells were harvested by centrifugation and serially diluted for further experiments.

Biosynthesis of SnO_2 NPs: Tin (II) chloride ($SnCl_2$) (1 mg) was used for an Sn^{2+} ion solution. The harvested *B. subtilis* cells (OD_{600}: 1.5) were resuspended in a 10 mL fresh LB medium and then 10 mL of $SnCl_2$ solution (1 mg mL^{-1}) was added. The mixed solution was incubated overnight in an anaerobic condition. The cells with the SnO_2 NPs were collected by centrifuging the solution at 3000 rpm for 5 min. Then, the sample was rinsed four times with deionized water (DIW) to purify it and the contaminants. The SnO_2 NP formation was verified by scanning electron microscopy with energy-dispersive X-ray spectroscopy (SEM/EDX).

SEM Analysis: The samples were treated with a 4% glutaraldehyde solution at 4 °C overnight, followed by thorough washing with a 0.1 M phosphate buffer saline (PBS) solution. Then, the samples were dehydrated using an ethanol series (35%, 50%, 70%, 90%, and 100%). The samples were examined using a field-emission scanning electron microscope (Supra 55 VP, Zeiss) for imaging their microstructure and morphology, and an EDX unit for the elemental analysis.

Preparation of Alginate-Based Packaging: Sodium alginate (2 g) was dissolved in 100 mL of DIW and stirred for 2 h. Then, 3 g of calcium chloride dihydrate was added to the solution and stirred for 2 h to prepare a homogenous hydrogel. A 0.1 M potassium ferricyanide ($K_3[Fe(CN)_6$) was added to the mixture and stirred gently for 24 h. To add sticky and adhesive properties to the tight packaging over the anode, a 4% glycerol was introduced. The sample was washed with DIW and mixed with 2% sodium hydroxide to allow the sample to be cross-linked. Finally, it was dried at 60 °C for 24 h.

Preparation of Germinant Powder: L-valine (10 mM) and AGFK (10 mM L-asparagine, 33.6 mM D-glucose, 33.6 mM D-fructose, 60 mM KCl) were mixed with an LB medium. The solution was first frozen at 50 °C for 3 h and then lyophilized in a freeze drier (FreeZone Plus 2.5 Liter Cascade Benchtop Freeze Dry System, Labconco, MO, USA) for 12 h. During the lyophilization, the chamber temperature was set to −25 °C and let back to room temperature gradually. The chamber pressure was 0.06 atm.

Fabrication of the Single MFC on Paper: A 2D sheet of Whatman 3 MM CHR filter paper was first prepared with hydrophobic wax boundaries using a commercial wax printer (Xerox Phaser, ColorQube 8570). The wax patterns on both sides of the paper and subsequent thermal treatment

at 150 °C for 30 s defined the anode and cathode. The wax was additionally printed on the cathode region to be used as an ion exchange membrane. A mixture of 2 mL poly(3,4-ethylenedioxythiophene):polystyrene sulfonate (PEDOT:PSS; 1 wt.%, Clevios PH1000, Heraeus, German) and 1 µL dimethyl sulfoxide (DMSO; D8418-100ML, Sigma–Aldrich, USA) was introduced into the patterned anodic region to be the highly conductive 3D environment. A mixture of 200 mg of silver oxide (Ag_2O; 11407–14, Alfa Aesar, USA) and 10 mL PEDOT:PSS was introduced to the patterned cathodic region. Ag_2O had been widely used as a cathodic catalyst for fuel cells. At the cathode, the electrons and protons, which were metabolically produced and flowed from the anode, could be combined with Ag_2O, generating Ag and water to enable the MFC operation. Graphite (Fisher Scientific Company, LLC, NC1044060) as the current collector was screen-printed on the anodic and cathodic compartments through a pre-patterned paper mask. Endospores (10 µL) with the biogenic NPs was pre-loaded on the engineered anodic area. Finally, the 2D sheet of the prepared paper was folded along the pre-defined crease to vertically align the anode, the ion-exchange membrane, and the cathode and then was attached with spray adhesive glue (3 M Super 77) to form an MFC.

Fabrication of the Six-MFC Stack on Paper: The fabrication of the six-MFC stack was based on the same steps of the single MFC with additional processes for packaging with the alginate and introduction of the germinant powder. For the serial connection of the individual MFCs, metallic paths were prepared by spraying nickel (MG Chemicals). For on-chip power demonstration in papertronics, an LED was mounted and connected to the MFC stack.

Electrical Measurement Setup: The electrical performance of the MFC was evaluated with a data acquisition system (DI-4108U, DataQ, USA) through various external resistors. The polarization curve and power output were obtained by measuring the voltage drops at selected external resistors (No resistor, 470, 250, 162, 100, 71, 47.5, 32, 22, 15, 10, 2, 1.5, 0.45, and 0.35kΩ), and calculating the corresponded current and power values. Power and current densities were normalized to the anodic area.

Electrochemical Measurement Setup: Cyclic voltammetry (CV) and electrochemical impedance spectroscopy (EIS) measurements were performed using a potentiostat (Squidstat Plus, Admiral Instruments). Anodic performance with various biocatalysts was assessed with a three-electrode electrochemical cell where a platinum foil and an Ag/AgCl in saturated KCl were used as a counter and a reference electrode, respectively. The CV performances were tested at a scan rate of 100 mV s^{-1} from −0.8 to 1.3 V voltage window. The EIS tests were operated under an excitation voltage of 0.5 V and scanning frequency from 0.1 Hz to 100 kHz.

Biodegradation Test: The biodegradation of the paper-based single MFC was assessed by studying its disintegration under a laboratory-scale composting condition. Tests were performed for a bacterial culture of *B. subtilis* (8 mL of 2 OD_{600} in LB medium). To facilitate biodegradation, the culture was replenished with a fresh LB medium daily. The weight loss of the MFC was measured weekly after rinsing with DIW and subsequently drying. Meanwhile, the biodegradation of the six-MFC stack was evaluated by being buried in the soil at the campus of the State University of New York at Binghamton (June 2023).

Statistical Analysis: All experimental data shown in this work were performed by repeating identical experiments at least three times. Data were represented as the mean ± standard errors of those experimental replicates.

Supporting Information

Supporting Information is available from the Wiley Online Library or from the author.

Acknowledgements

This work was supported by the National Science Foundation (ECCS #2246975) and the Office of Naval Research (#N00014-21-1-2412).

Conflict of Interest

The authors declare no conflict of interest.

Data Availability Statement

The data that support the findings of this study are available from the corresponding author upon reasonable request.

Keywords

Bacillus subtilis, biodegradability, biogenic nanoparticles, paper-based microbial fuel cells, papertronics, transient electronics

Received: August 9, 2023
Revised: September 11, 2023
Published online: October 3, 2023

[1] M. R. Hasan, P. Sharma, S. Suleman, S. Mukherjee, E. G. Celik, S. Timur, R. Pilloton, J. Narang, *ACS Appl. Bio Mater.* **2023**, *6*, 1368.
[2] M. Landers, A. Elhadad, M. Rezaie, S. Choi, *ACS Appl. Mater. Interfaces* **2022**, *14*, 45658.
[3] M. M. Hamedi, A. Ainla, F. Güder, D. C. Christodouleas, M. T. Fernández-Abedul, G. M. Whitesides, *Adv. Mater.* **2016**, *28*, 5054.
[4] M. Mohammadifar, S. Choi, *Adv. Mater. Technol.* **2017**, *2*, 1700127.
[5] W. Li, Q. Liu, Y. Zhang, C. Li, Z. He, W. C. H. Choy, P. J. Low, P. Sonar, A. K.o K.o Kyaw, *Adv. Mater.* **2020**, *32*, 2001591.
[6] A. Suresh Khurd, B. Kandasubramanian, *Carbohydr. Polym. Technol. Appl.* **2022**, *4*, 100234.
[7] Z. Su, Y. Yang, Q. Huang, R. Chen, W. Ge, Z. Fang, F. Huang, X. Wang, *Prog. Mater. Sci.* **2022**, *125*, 100917.
[8] R. Martins, D. Gaspar, M. J. Mendes, L. Pereira, J. Martins, P. Bahubalindruni, P. Barquinha, E. Fortunato, *Appl. Mater. Today* **2018**, *12*, 402.
[9] I. Cunha, J. Martins, P. G. Bahubalindruni, J. T. Carvalho, J. Rodrigues, S. Rubin, E. Fortunato, R. Martins, L. Pereira, *Adv. Mater. Technol.* **2021**, *6*, 2100633.
[10] M. M. Hamedi, V. E. Campbell, P. Rothemund, F. Güder, D. C. Christodouleas, J.-F. Bloch, G. M. Whitesides, *Adv. Funct. Mater.* **2016**, *26*, 2446.
[11] D. Tobjork, R. Osterbacka, *Adv. Mater.* **2011**, *23*, 1935.
[12] A. C. Siegel, S. T. Phillips, M. D. Dickey, N. Lu, Z. Suo, G. M. Whitesides, *Adv. Funct. Mater* **2010**, *20*, 28.
[13] J. Liu, C. Yang, H. Wu, Z. Lin, Z. Zhang, R. Wang, B. Li, F. Kang, L. Shi, C. P. Wong, *Energy Environ. Sci.* **2014**, *7*, 3674.
[14] S. Nandy, S. Goswami, A. Marques, D. Gaspar, P. Grey, I. Cunha, D. Nunes, A. Pimentel, R. Igreja, P. Barquinha, L. Pereira, E. Fortunato, R. Martins, *Adv. Mater. Technol.* **2021**, *6*, 2000994.
[15] M. P. Cenci, T. Scarazzato, D. D. Munchen, P. C. Dartora, H. M. Veit, A. M. Bernardes, P. R. Dias, *Adv. Mater. Technol.* **2022**, *7*, 2001263,.
[16] T. Juqu, S. C. Willenberg, K. Pokpas, N. Ross, *Adv. Sens. Energy Mater.* **2022**, *1*, 100037
[17] T. H. Nguyen, A. Fraiwan, S. Choi, *Biosens. Bioelectron.* **2014**, *54*, 640.
[18] Y. Gao, S. Choi, *Adv. Mater. Technol.* **2017**, *2*, 1600194.
[19] Y. Gao, S. Choi, *Adv. Mater. Technol.* **2018**, *3*, 1800118.
[20] K. Rajaram, S. M. Yang, S. Hwang, *Adv. Energy Sustainability Res.* **2022**, *3*, 2100223.
[21] M. Mohammadifar, I. Yazgan, J. Zhang, V. Kariuki, O. Sadik, S. Choi, *Adv. Sustainable Syst.* **2018**, *2*, 1800041.

[22] Y. Gao, M. Mohammadifar, S. Choi, *Adv. Mater. Technol.* **2019**, *4*, 1970039.
[23] S. Choi, *Small* **2022**, *18*, 2107902.
[24] S. Choi, *Batteries* **2023**, *9*, 119.
[25] M. Mohammadifar, S. Choi, *J. Power Sources* **2019**, *429*, 105.
[26] M. Landers, S. Choi, *Nano Energy* **2022**, *97*, 107227.
[27] M. Rezaie, Z. Rafiee, S. Choi, *Adv. Energy Mater.* **2023**, *13*, 2202581.
[28] M. Rezaie, S. Choi, *Small* **2023**, *19*, 2301135
[29] G. Pankratova, D. Leech, L. Gorton, L. Hederstedt, *Biochemistry* **2018**, *57*, 4597.
[30] G. Christie, P. Setlow, *Cell. Signaling* **2020**, *74*, 109729.
[31] L. M. González, N. Mukhitov, C. A. Voigt, *Nat. Chem. Biol.* **2020**, *16*, 126.
[32] B. E. Logan, R. Rossi, A. Ragab, P. E. Saikaly, *Nat. Rev. Microbiol.* **2019**, *17*, 307.
[33] B. Cao, Z. Zhao, L. Peng, H.-Y. Shiu, M. Ding, F. Song, X. Guan, C. K. Lee, J. Huang, D. Zhu, X. Fu, G. C. L. Wong, C. Liu, K. Nealson, P. S. Weiss, X. Duan, Y. Huang, *Science* **2021**, *373*, 1336.
[34] R. Wang, H. Li, J. Sun, L. Zhang, J. Jiao, Q. Wang, S. Liu, *Adv. Mater.* **2021**, *33*, 2004051.
[35] L. Liu, S. Choi, *J. Power Sources* **2021**, *506*, 230251.
[36] M. Chen, X. Zhou, X. Liu, R. J. Zeng, F. Zhang, J. Ye, S. Zhou, *Biosens. Bioelectron.* **2018**, *108*, 20.
[37] Y. T. Gebreslassie, H. G. Gebretnsae, *Nanoscale Res. Lett.* **2021**, *16*, 97.
[38] S. Sagadevan, J. A. Lett, I. Fatimah, Y. Lokanathan, E. Léonard, W. C. Oh, M. A. M. Hossain, M. R. Johan, *Mater. Res. Express* **2021**, *8*, 082001.
[39] E. Eymard-Vernain, S. Luche, T. Rabilloud, C. Lelong, *Sci. Rep.* **2018**, *8*, 2978.
[40] E. P. Riley, C. Schwarz, A. I. Derman, J. Lopez-Garrido, *Microb. Cell* **2021**, *8*, 1.
[41] A. Klinkova, P. De Luna, E. H. Sargent, E. Kumacheva, P. V. Cherepanov, *J. Mater. Chem. A* **2017**, *5*, 11582.
[42] X. Xu, F. Zhao, N. Rahunen, J. R. Varcoe, C. Avignone-Rossa, A. E. Thumser, R. C. Slade, *Angew. Chem., Int. Ed.* **2011**, *50*, 427.
[43] A. P. Adebule, B. I. Aderiye, A. A. Adebayo, *Ann. Appl. Microbiol. Biotechnol. J.* **2018**, *2*, 1.
[44] L. Zhuang, S. Zhou, *Electrochem. Commun.* **2009**, *11*, 937.
[45] Y. Gao, J. H. Cho, J. Ryu, S. Choi, *Nano Energy* **2020**, *74*, 104897.
[46] D. R. Lovley, J. D. Coates, *Curr. Opin. Biotechnol.* **1997**, *8*, 285.
[47] T. Klaus-Joerger, R. Joerger, E. Olsson, C.-G. Granqvist, *Trends Biotechnol.* **2001**, *19*, 15.
[48] T. Ozawa, D. T. Nguyen, K. Taguchi, *Journal of Engineering and Science Research* **2017**, *1*, 197.
[49] J. Ryu, M. Landers, S. Choi, *Biosens. Bioelectron.* **2022**, *205*, 114128.